Development of a MATLAB/Simulink Model of a Single-Phase Grid-Connected Photovoltaic System

Michael E. Ropp, *Member, IEEE*, and Sigifredo Gonzalez

***Abstract*—Because of their deployment in dispersed locations on the lowest voltage portions of the grid, photovoltaic (PV) systems pose unique challenges to power system engineers. Computer models that accurately simulate the relevant behavior of PV systems would thus be of high value. However, most of today's models either do not accurately model the dynamics of the maximum power point trackers (MPPTs) or anti-islanding algorithms, or they involve excessive computational overhead for this application. To address this need, a MATLAB/Simulink model of a single-phase grid-connected PV inverter has been developed and experimentally tested. The development of the PV array model, the integration of the MPPT with an averaged model of the power electronics, and the Simulink implementation are described. It is experimentally demonstrated that the model works well in predicting the general behaviors of single-phase grid-connected PV systems. This paper concludes with a discussion of the need for a full gradient-based MPPT model, as opposed to a commonly used simplified MPPT model.**

***Index Terms*—Inverters, islanding detection, modeling and simulation, photovoltaics (PVs).**

I. Introduction

PHOTOVOLTAIC (PV) systems produce electricity without producing CO_2. This property has led to worldwide government policies aimed at increasing the deployment of grid-connected PV systems that are connected with, and can export power to, utility power networks. PV systems are usually deployed in a highly dispersed mode, in the lowest voltage portions of the grid (down to residential end-use voltages), and they thus present unusual challenges for power system engineers tasked with understanding how high penetration levels of PV in industrial parks or "solar subdivisions" might impact system operations. A well-verified computer model would be of great help in this task.

In order to meet the needs described earlier, a number of important aspects of PV inverters need to be modeled with reasonable accuracy. These include the following.

1) *Islanding detection behavior*: A suitable model must reasonably simulate the inverters' means of islanding detection. Islanding detection is discussed thoroughly in the literature [1], [2], and applicable standards, such as IEEE-1547, UL-1741, and IEC-62116, require that a grid-connected PV inverter be able to detect and prevent unintentional islanding [3]–[5]. The standards suggest the use of a specific test to demonstrate that a PV inverter can meet this requirement and be certified as a "nonislanding inverter," but this test is difficult and somewhat expensive to perform in spite of its conceptual simplicity, and thus, modeling could also be of help in understanding the results of anti-islanding tests.
2) *Action of the maximum power point tracker* (*MPPT*): The MPPT is effectively the amplitude controller for the inverter's output, and its operation can strongly affect system behavior [6] and must also be properly simulated. In addition, the interaction between the MPPT and the large buffer capacitor usually used at the dc inputs of PV inverters is important and should be simulated.
3) *Response to grid voltage and frequency fluctuations*: For PV inverters, this primarily means that the trips for abnormal voltages or frequency must be simulated.

PV system models for use in power system simulations have been reported by other authors (for example, [7]–[9]). Although useful in some cases, most of these suffer from one of the following problems.

1) They use full switching models of the converter that impose too high of a computational burden for the model to be useful in power system simulations.
2) They do not model the anti-islanding controls.
3) They do not realistically capture the dynamics introduced by the PV array, input buffer capacitor, and MPPT.

This paper describes the work undertaken to produce a model that meets this need. The paper has two goals. First, it presents the model itself and describes the extensive experimental validation conducted in collaboration with the Distributed Energy Technologies Laboratory (DETL) at Sandia National Laboratories, Albuquerque, NM. Second, after the model is vetted, it is used to examine the need for the complex MPPT model used here.

II. Description of the Model

A. Overview

The system being modeled is shown in Fig. 1. It consists of a PV array feeding an H-bridge inverter (switches S_1–S_4) that feeds current into the utility voltage V_u through an equivalent interconnecting inductance $L_{\rm eq}$ that includes effects from output filters, transformers, and the utility source impedance. The power output of single-phase inverters oscillates at twice the line frequency, and thus, a large buffer capacitor C_b is included between the PV and the H-bridge.

Manuscript received May 30, 2007; revised February 20, 2008. This work was supported in part by the National Science Foundation under Grant ECS-0238533. Paper no. TEC-00205-2007.

M. E. Ropp is with the Department of Electrical Engineering, South Dakota State University, Brookings, SD 57007 USA, on leave from Sandia National Laboratories, Albuquerque, NM 87185 USA (e-mail: michael.ropp@ieee.org).

S. Gonzalez is with the Distributed Energy Test Laboratory, Sandia National Laboratories, Albuquerque, NM 87185 USA (e-mail: sgonza@sandia.gov).

Color versions of one or more of the figures in this paper are available online at http://ieeexplore.ieee.org.

Digital Object Identifier 10.1109/TEC.2008.2003206

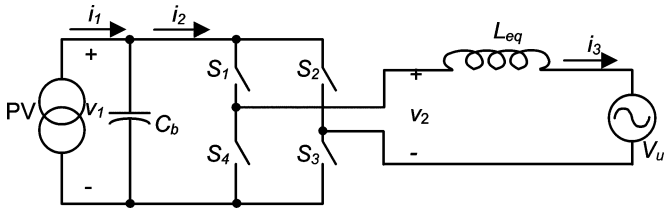

Fig. 1. Schematic of the system being modeled.

The model includes:

1) six islanding detection algorithms:
   a) Sandia frequency shift (SFS) [10];
   b) the classical linear instability (CLI) method [11], [12];
   c) Sandia voltage shift (SVS) [2];
   d) rate of change of frequency (RoCoF) [13];
   e) impedance detection [1], [2];
   f) frequency bias [10];
2) two I–V curve based-models of a PV array;
3) a perturb-and-observe (P&O) MPPT [14];
4) an s-domain representation of an L–C output filter.

This model is unique in its inclusion of CLI and in its ability to use any of the anti-islanding methods in combination (which is common in practice), except for CLI and SFS.

B. MPPT

The PV array, capacitor C_b, and MPPT are usually modeled in one of two ways for power system simulations: as a Thevenin equivalent or as a constant-power source regulated by a classical feedback loop. These models have two major advantages: high computational efficiency and the lack of a need for a detailed PV model. However, virtually all real PV inverters use MPPT algorithms that belong to the family of gradient-based optimization methods [15]. The most common of these is the P&O method, which is a variant of the simple 1-D gradient-based minimization technique. Modeling this type of MPPT using a simplified model might be problematic for two main reasons.

1) The dynamics of gradient-based controls and the linear controller are inherently different [15].
2) The linear controller MPPT model does not model the PV array and capacitor C_b, and thus, cannot properly simulate the energy-limited nature of the source.

Thus, in this paper, a P&O MPPT model along with a model of the PV array and capacitor was implemented. The PV + capacitor model is covered in the next section. A block diagram of the P&O MPPT model developed here is shown in Fig. 3. This model implements a basic 1-D gradient search with a fixed step size [15]. The instantaneous PV inverter ac output current (i_3 in Fig. 1 and IPV in Fig. 3) and the point of common coupling voltage (v_u in Fig. 1 and VPCC in Fig. 3) are multiplied to obtain the inverter output power, which is averaged over a time window of one-tenth of the user-defined MPPT stepping interval. The PV power measurement passes through a zero-order sampling block. The "Integer Delay" block holds the sampled power for one stepping interval, so that the "Subtract" block subtracts the present power reading from the previous, to get the algebraic sign of the change in power. That sign is used to set a flag in the block labeled "Convert CtZ block output"; if the change in power is positive (output of "Compare To Zero" block is 1), the flag is set to $+1$, and if negative or zero (output of "Compare To Zero" block is 0), the flag is set to -1. The flag then multiplies a user-settable MPPT increment, which, in turn, is added to the present PV + capacitor current to increment or decrement it as appropriate.

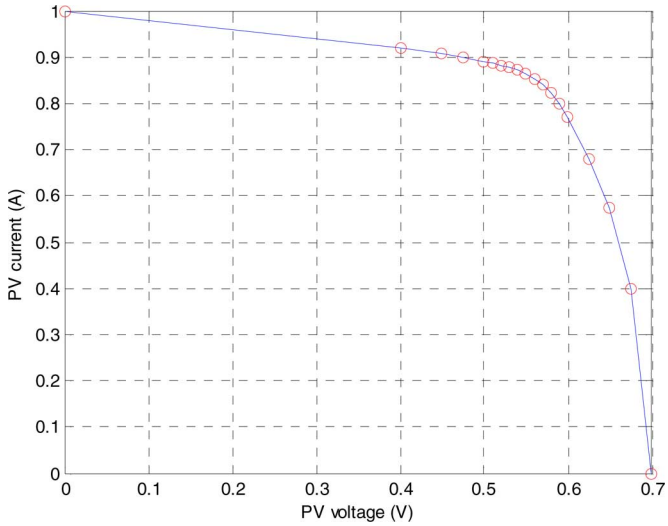

Fig. 2. Plot of the "unit I–V curve" used in the model.

C. PV Array Model

Modeling the PV array in this context is always a challenge. The physical I–V relationship based on the Shockley equation requires parameters that are rarely available to power electronics or power system engineers and is thus unsuitable. Mathematical curve fits are available, but most of these are cumbersome to use in this application.

To achieve accuracy while minimizing computational burden and maintaining simplicity for the user, this model gives the user two options for modeling the PV array. The first is a highly simplified approach based on the "unit" I–V curve shown graphically in Fig. 2 and in tabular form in Table I, developed by the authors of this paper to approximately represent the I–V curve of a single generic PV cell, except for the fill factor of 0.682, which is more representative of an array.

This "unit" curve is scaled to any arbitrary system size by entering the open-circuit voltage at standard test conditions (STC) and the nominal STC power of the array, so the user need know only these two parameters. The I–V curve can be changed to more closely represent a particular array by changing the vectors used in the lookup table.

This approach is useful for most system-level applications, but it has one important drawback: it fixes the fill factor (FF), which in reality depends on irradiance and temperature. Because the FF affects MPPT performance, a second PV array modeling option is included, i.e., of accepting I–V curve data from a program such as "Sandia IVTracer2" that generates accurate

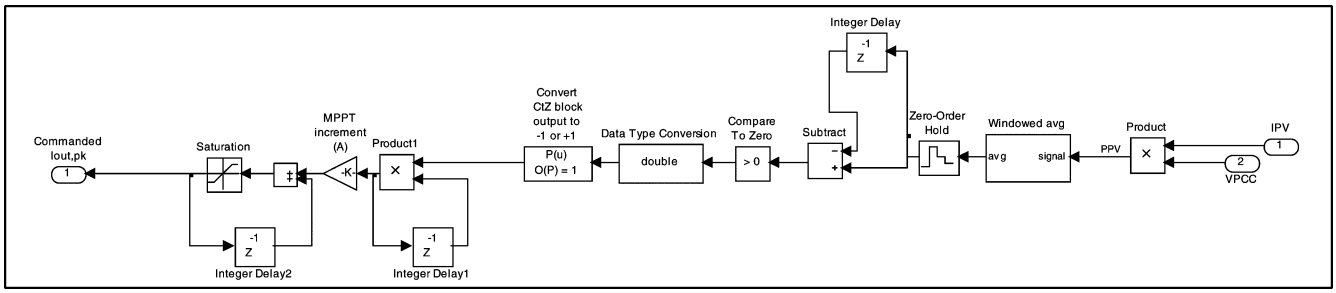

Fig. 3. Perturb-and-observe maximum power point tracker. Signal propagation is from right to left (the inputs are at the right).

TABLE I
VALUES USED IN THE "UNIT I–V CURVE" LOOKUP TABLE

Voltage (V)	Current (A)
0.0	1.0
0.4	0.92
0.45	0.907
0.475	0.9
0.5	0.89
0.51	0.886
0.52	0.882
0.53	0.8775
0.54	0.872
0.55	0.864
0.56	0.853
0.57	0.84
0.58	0.8225
0.59	0.8
0.6	0.77
0.625	0.68
0.65	0.575
0.675	0.4
0.7	0.0

I–V curves from an extensive database of measured module parameters. The Simulink model that implements this latter PV array model for three different irradiances is shown in Fig. 4. The user copies and pastes into the I and V blocks the current and voltage vectors at different irradiances from IVTracer2. The "Subtract" block implements Kirchhoff's current law at the node at the top of capacitor C_b in Fig. 1; it subtracts the load current from the PV current (i_1–i_2). The resulting capacitor current is used to compute the capacitor voltage via the 1/capacitance and "Integration by the capacitor" blocks. The capacitor and PV voltage are the same (v_1 in Fig. 1), so the capacitor voltage is fed back into the I–V lookup table.

D. Anti-Islanding Methods

One distinguishing feature of this model is that it combines the realistic MPPT model with models of six anti-islanding methods. Fig. 5 shows the implementation of one of these, SFS and frequency bias. This implementation is somewhat novel in that it uses the phase-locked loop (PLL) that produces the sine wave reference for the inverter's output current, which modestly improves the computational speed over lookup-table-based versions. Over/undervoltage and over/underfrequency relaying are also modeled.

E. Modeling of the Power Stage

The model would not be useful for system simulations if a full switching model of the power stage were used, because simulation times and data file sizes would be excessive. Instead, an average model of the power stage was used, and for the hysteresis-controlled H-bridge, this model is merely a gain. However, one challenge that had to be overcome in this research was how to integrate this averaged model with the MPPT model described earlier.

The approach developed here is as follows. Output power control is discussed here because all of the converter's dynamics are in the MPPT feedback loop, making it the more complex case (input power control is also available). Since the output current (i_3 in Fig. 1) feeds into an essentially constant utility voltage source, increasing i_3 will always result in an increase in output power. Thus, the MPPT will command ever-increasing currents until the process becomes limited by the gain of the power stage. At that point, even though the MPPT commands an increase in current, the output current will actually decrease, the output power will fall, and the P&O MPPT will reverse direction. The gain of the power stage is clearly a function of voltage v_1 in Fig. 1, and that functional dependency must be modeled. There are two ways to approach this problem. The first is to recognize that the H-bridge inverter is a buck-type converter. If one considers a PWM buck dc–dc converter, the relationship of output current to input voltage can be determined as follows:

$$\frac{v_o}{v_i} = D = \frac{Z i_o}{v_i}$$
$$i_o = v_i \frac{D}{Z} \tag{1}$$

where the input voltage v_i is the converter's input voltage, v_o is the converter's output voltage, i_o is the output current, Z is the impedance of the load fed by the converter, and D is the duty ratio. The output current is proportional to the input voltage. In the present case, the load is not simply an impedance but rather a nonideal (Thevenin) voltage source, the determination of Z is nontrivial, and D would not be constant.

Another approach would be to consider that in the hysteresis-controlled H-bridge inverter, the current i_3 in Fig. 1 is controlled using the H-bridge to apply $\pm v_1$ at v_2, thereby controlling the time rate of change of the current through L_{eq}. Consider the case in which the PV array is nearing maximum power operation after

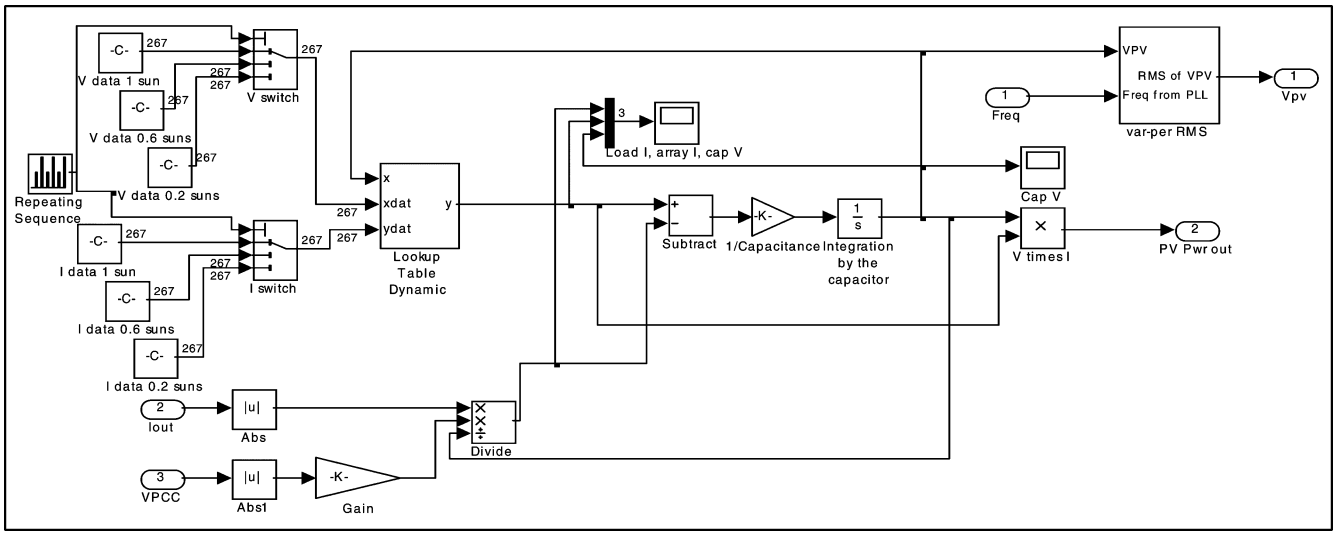

Fig. 4. Block diagram of the PV array model. Note that "$I_{\rm out}$" is the inverter output current and is an input here.

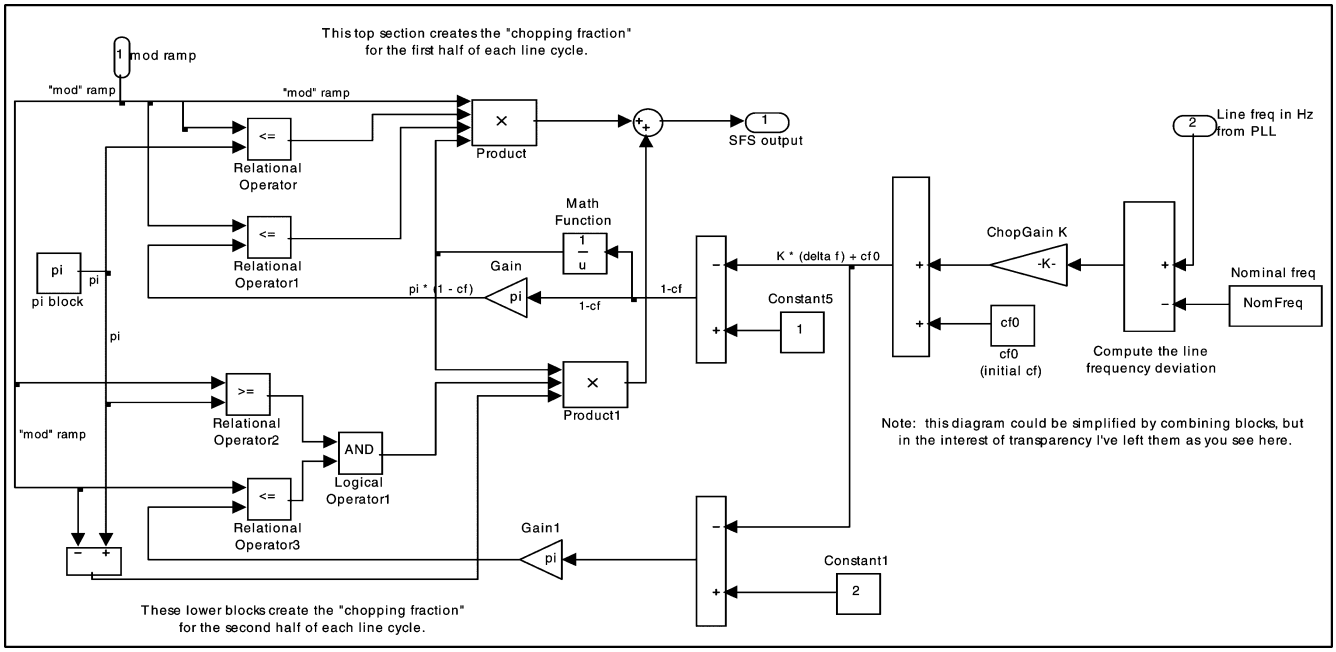

Fig. 5. SFS waveform generator. Signal propagation is from right to left (the input is at the right).

starting from zero current. The current i_3 is increasing, and the voltage v_1 has fallen to the point at which the converter cannot further increase the amplitude of the current. This case will appear approximately as shown in normalized form in Fig. 6, which shows the sine wave reference used by the hysteresis controller, the hysteresis boundaries, and a linear approximation to the sine wave at $t = 0$. The PV voltage becomes so low that the current through $L_{\rm eq}$ "ramps" at approximately the same rate as the reference sine wave, and the bridge does not switch at all during the first portion of the sine wave. Under this condition, near the beginning of the sine wave ($t = 0$), the derivative of i_3 can be expressed as

$$\frac{di_3}{dt} = \frac{v_2 - v_U}{L_{\rm eq}} \approx \omega I_{3m} \cos \omega t \tag{2}$$

where ω is the frequency of v_U (in radians per second) and I_{3m} is the maximum value of i_3 (in Amperes). The approximation is acceptable near the beginning of the cycle of the sine wave, and as long as the hysteresis bandwidth is small. Combining these equations and considering the case of $t = 0$ allows a calculation of the maximum amplitude of the current as a function of the PV voltage

$$I_{3m} = \frac{v_{\rm PV}}{\omega L_{\rm eq}}. \tag{3}$$

This calculated value of I_{3m} will actually be above the true value, but the relationship again supports the notion that it is physically reasonable to make the converter gain proportional to v_1, with the constant of proportionality being somewhat less

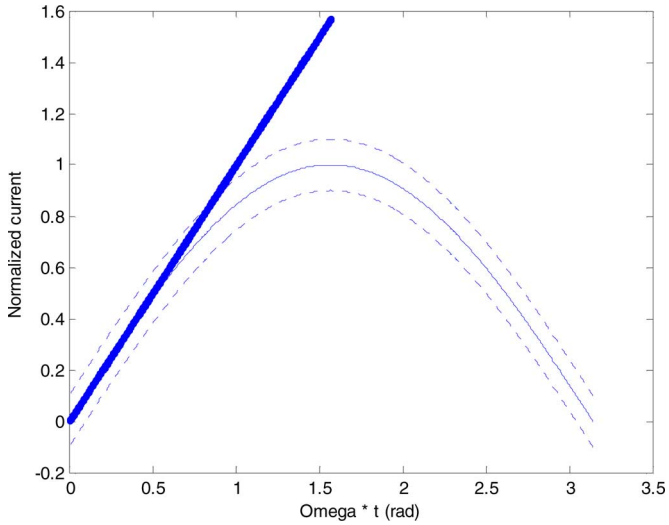

Fig. 6. Plot of normalized reference current waveform for hysteresis control (solid light line), hysteresis bands (dashed light lines), and straight-line approximation to the reference at $t = 0$ (heavy solid line).

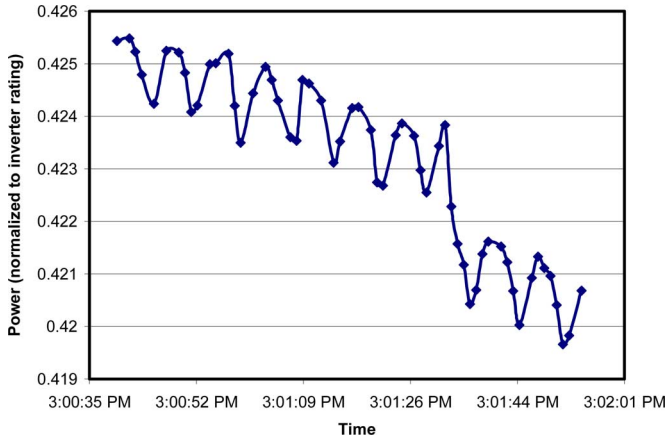

Fig. 7. Experimentally measured MPPT power ripple.

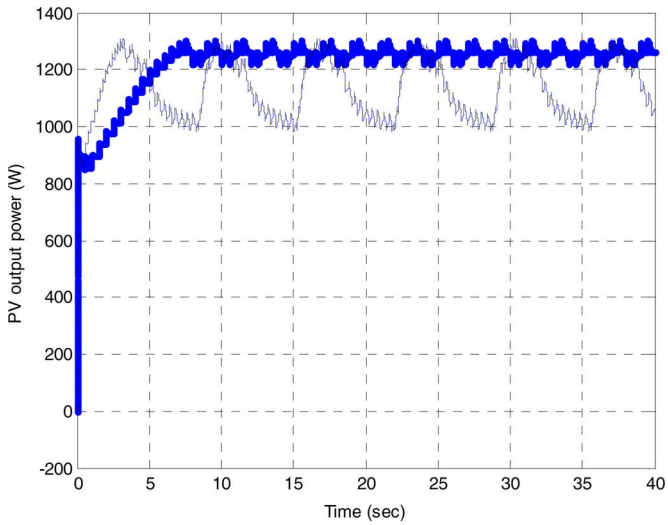

Fig. 8. Effect of MPPT decision rate on PV output power, for fixed capacitor size and MPPT increment.

than that given by (3). The approach followed in the model being discussed here was to normalize I_{3m} by its maximum value, which would be attained if the PV array reached its open-circuit voltage $V_{\rm OC}$, and multiply by a gain constant K:

$$I_{3m,\rm norm} = K\frac{v_1}{V_{\rm OC}}. \tag{4}$$

Now, explicit knowledge of $L_{\rm eq}$ is not required. A value of $K = 3$ has proven to be reasonable for most system-level work, but if higher accuracy is desired, the value of K can be adjusted until the maximum power increment specified by the user is of appropriate size, near the beginning of a simulation started from zero initial conditions.

III. Model Validation

One feature that sets this model apart from others in the literature is the level to which it has been experimentally vetted. The model was extensively tested by comparing model results against experimentally obtained data from the Distributed Energy Technologies Laboratory (DETL) at Sandia National Laboratories. A number of test cases have been examined, a few of which will be presented here.

A. Effect of MPPT Decision Rate on MPPT Stability

It is known that some PV inverters exhibit a considerable low-frequency ripple because of the time lag required for the PV array + capacitor to reach its new operating point when the MPPT perturbs the operating state. This can reduce steady-state MPPT efficiency and lead to undesired shutdowns during changing irradiance conditions, but it can also reduce run-on times during islanding tests. Fig. 7 shows an experimentally measured example; the vertical axis indicates the power output as a percent of nameplate rating. There is approximately a 0.3% MPPT ripple in this example, at a frequency of about 0.15 Hz. The general downward slope is due to changing irradiance.

The model was tested to see whether it correctly predicted this behavior. A representative example is shown in Fig. 8. In this simulation, the PV array's maximum power was 1265 W, irradiance was fixed, and the size of C_b was 40 mF. The heavy trace was produced using an MPPT stepping rate of 2 Hz (MPPT stepping time interval of 0.5 s), and the lighter trace was produced using an MPPT stepping rate of 5 Hz. If the MPPT steps too quickly, the low-frequency oscillation evident in the lighter trace in Fig. 8 begins to appear, i.e., the model predicts the onset of undesired oscillation as the MPPT stepping time interval is increased. If the rate increases too far—in this case, 10 Hz was sufficient—the MPPT becomes unstable. Similar behavior could be observed if the MPPT stepping time interval was fixed but the buffer capacitor size was increased. This is consistent with known inverter behavior, suggesting the MPPT model is realistic.

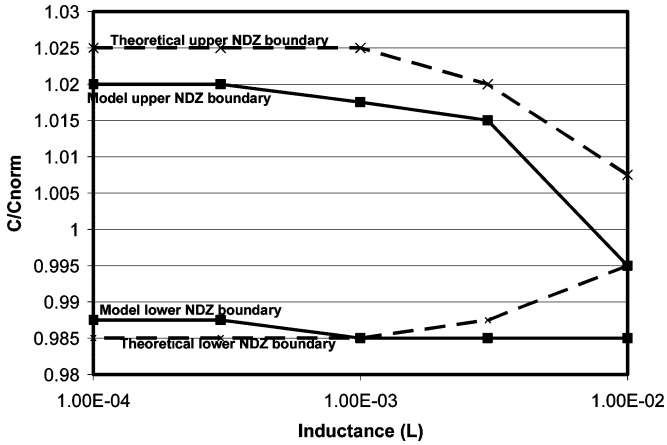

Fig. 9. Comparison of the NDZ for SFS predicted by the phase criterion ("theoretical," marked by dashed lines) and by the model (heavy lines with squares).

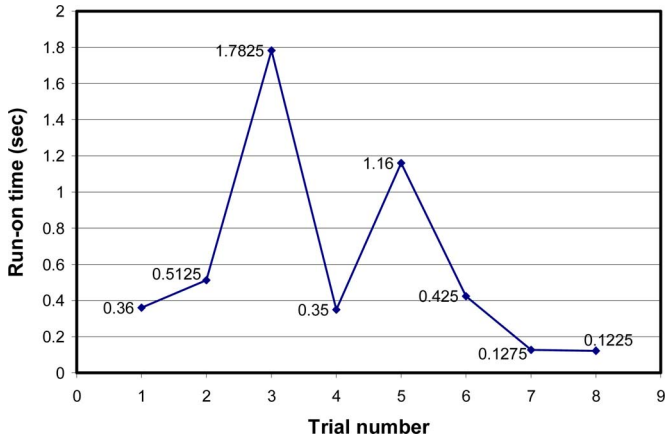

Fig. 10. Average run-on times for four SFS inverters at full power (experimental result).

B. Anti-Islanding Method Nondetection Zones and Behavior as a Function of Load Quality Factor

The modeled islanding prevention schemes have been thoroughly tested by comparison with both earlier theoretical work and laboratory results. In general, the anti-islanding models appear to work well, predicting general behaviors and nondetection zones (NDZs) reasonably accurately.

Fig. 9 shows the results of one set of tests to determine the NDZs predicted by theory (phase criteria [16]) and the model. The purpose of the test was to see how accurately the model predicted the location of the edge of the NDZ. The SFS gain was 0.05, the load was a parallel *RLC* with $R = 11.8\ \Omega$, and the MPPT was turned "off". Fig. 9 shows generally reasonable agreement, but there are two discrepancies apparent: the model NDZ is slightly shifted downward from the theoretical one, and the trend in the model's lower boundary appears to be inverted from expectations. The downward shift is attributed to the fact that the model's simulated inverter output current lags the voltage by about 2°. That phase shift comes from the inverter's output low-pass filter, which was left as-is because it and its phase shift are representative of "real-world" inverters.

The reason for the lower boundary discrepancy appears to lie within the PLL used to synchronize the inverter's current reference wave to the utility voltage. The Q-factors of loads toward the left side of Fig. 9 are very high, resulting in an inevitable phase "glitch" upon loss of utility. The PLL senses this phase jump and adjusts its frequency in an attempt to maintain phase lock, resulting in a frequency transient that includes an overshoot. For L-values of 300 and 100 μH (the leftmost two values in Fig. 9), the overshoot for C_{norm}-values less than 0.9875 is large enough to result in an over-frequency trip. The same effect does not appear for the upper boundary because of the asymmetry of the frequency trip limits; the PLL transient exceeds the 60.5-Hz limit on the high side but does not quite reach the 59.3-Hz limit on the low side.

C. Using the Model to Understand an Observed Interaction Between Islanding Prevention and MPPT Functions

This test was described in an earlier paper [9]. The model was used to help explain an experimental observation that a particular commercially available PV inverter did not island when its MPPT was active, but islanded readily for certain loads when the inverter deactivated its MPPT due to excessive temperature or input power. The model demonstrated that the reason was that the MPPT was marginally stable, so that when the utility was lost, the actual mechanism by which islanding was detected was that the perturbation caused by the anti-islanding algorithm destabilized the MPPT, eventually leading to an input low-voltage cutoff.

D. Comparison of Modeled and Experimental Results in a Multiinverter Test

Here, we describe a use of the model to address a question that to the best of our knowledge has not been addressed in the literature to date. One issue of concern to utility planners is the high-penetration case, where the total power rating of a number of small independent PV systems connected to a given portion of the utility system is a significant fraction of the power capacity of that section of the utility. One worry about the high-penetration case is that the loss-of-mains detection systems of the various PV systems may interfere with each other in such a way that they lose effectiveness.

To address this, a high-penetration experiment was carried out at the Distributed Energy Test Laboratory at Sandia National Laboratories. This test involved four 2.5-kW PV inverters using both SFS and SVS and feeding a common *RLC* load with a Q of 2.5, tuned to resonate at 60 Hz. The results of the full-power tests are shown in Fig. 10.

In each individual test, the run-on times of the four inverters were tightly clustered, but between tests, there was a very broad variability. In some cases, the inverters shut down within ten line cycles, but in one case, the inverters ran on for over 100 cycles and came close to exceeding the 2-s limit allowed by IEEE-1547. (In no case did they actually exceed that limit.)

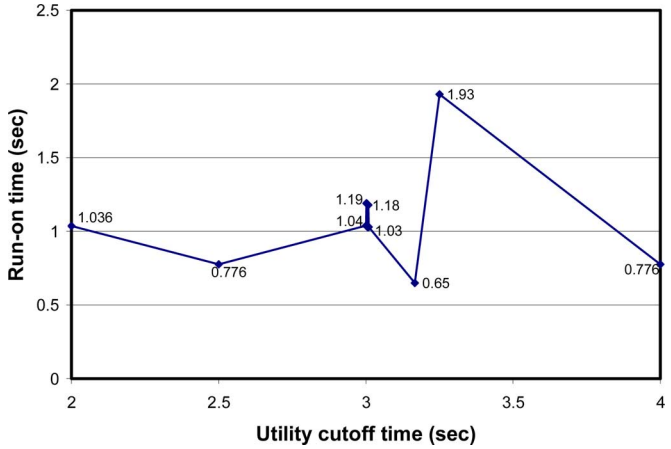

Fig. 11. Results of simulations of four inverters in which the utility cutoff time was varied, with all inverter and load parameters fixed.

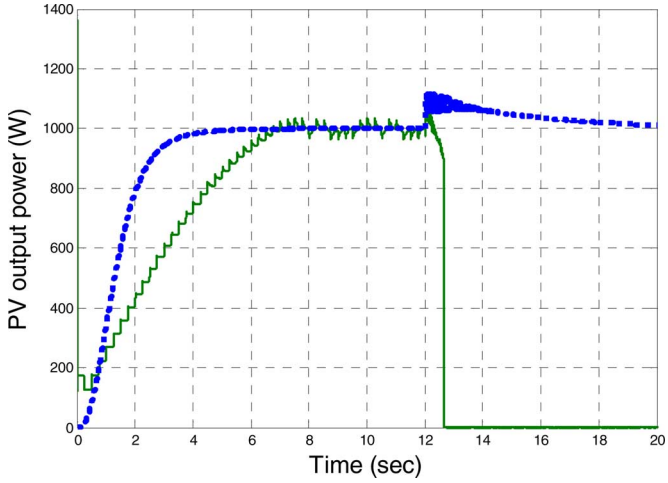

Fig. 12. Simulations of two SVS anti-islanding tests: one using a linear controller-based MPPT simulation (heavy dashed trace) and one using the gradient-based MPPT model described here (lighter solid trace).

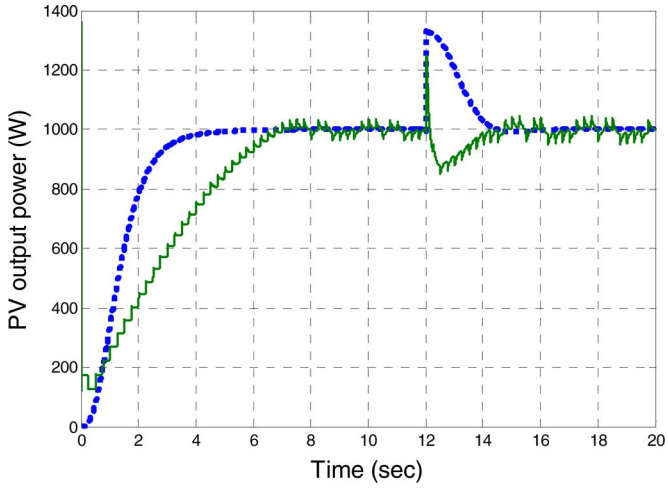

Fig. 13. Two simulated inverters with SVS during a utility voltage transient. One inverter uses a linear controller MPPT simulation (heavy dashed trace); the other uses the gradient-based MPPT model described here (lighter solid trace).

This variability is an indication of how difficult this test is to control completely, and also of the complexity of the interactions between the two anti-islanding methods and the MPPT. However, interpretation of the results is difficult and controversial. Which of the variety of run-on times is most representative of the inverters' performance in this situation?

This four-inverter case was simulated using the model presented in this paper. The inverters were connected in parallel, without interconnecting impedances, and the parameters were set as follows:

$V_{u,\mathrm{norm}} = 240$ Vrms
$R = 5.76\,\Omega$ $L = 6.115$ mH $C = 1.1513$ mF
MPPT stepping interval $= 0.25$ s MPPT increment $= 2$
SFS gain $= 0.0185$ SVS gain $= 0.01$.

Then, a number of simulations were run to study the effects of varying several parameters. One of the most interesting results was obtained when varying the time at which the utility was disconnected over the range of 2–4 sec. The results of this set of simulations are shown in Fig. 11. The horizontal-axis variable in Fig. 11 is the time at which the utility was disconnected, with $t = 0$ being the start of the simulation. A number of closely spaced simulations were run near 3 s to investigate the effect of cutting the utility off at different points in the sine wave. Fig. 11 suggests that this factor made only a small difference, but when a larger time step was used, corresponding to different locations within the interacting cycles of SFS, SVS, and the MPPT, it was found that the run-on time variation was only due to changing the utility cutoff time varied by almost a factor of 3, from 0.65 to 1.93 s. The maximum run-on time and range of run-on times predicted by the model are reasonably close to those measured in the experiments. Figs. 10 and 11 suggest that all of the run-on times found during the experiment are characteristic of the combination of inverters, and supports the test protocols specified in UL-1741, IEEE-1547, and IEC-62116 that use as their benchmark the longest run-on time obtained over several tests. This case also demonstrates the value of the model; without this "virtual laboratory," it would be difficult to gain an understanding of the behavior in Fig. 10, because it is caused by interactions that are difficult to isolate experimentally.

IV. Comparison of MPPT Modeling Methods

After the model was well verified, it was used to examine the aforementioned concern about potential differences between the linear controllers typically used to model MPPTs in large system simulations and the actual gradient-based MPPTs in real converters. In many cases, the linear MPPT model actually worked well, but many problems also became apparent. Although anomalies were found for many combinations of inverter functions, simulations involving the SVS method were particularly problematic. Two representative results are shown in Figs. 12 and 13. Fig. 12 shows two SVS anti-islanding simulations, one with the linear controller (heavy dashed trace) and one with the gradient-based MPPT (lighter solid trace). The utility is lost at $t = 12$ s. The linear controller runs on indefinitely, in

part because it does not model the energy-limited nature of the source and in part because its output does not contain the MPPT perturbations, but the gradient-based inverter shuts down fairly quickly. In this case, the linear MPPT can lead to erroneous conclusions.

Fig. 13 shows simulations of the same two inverters during a utility voltage transient, with the SVS anti-islanding method active. At time $t = 12$ s, the utility voltage undergoes a step decrease from 120 to 110 V_{rms}. The inverters are identical except for the MPPT model. Because the energy constraints on the PV + capacitor source are not modeled, the simulated SVS using the linear MPPT model increases the output voltage much more than it would be able to in reality. The response of the energy-constrained gradient-based MPPT, which does model the PV + capacitor, is smaller and in the opposite direction. The model without the energy constraint could lead to erroneous conclusions about such things as the impact of high penetrations of PV during system transients.

V. Conclusion

This paper presents an accurate behavioral model of a grid-tied PV system suitable for system-level investigations. Simplified means for modeling the PV array and integrating a gradient-based MPPT into a very simple averaged model of the power converter are developed, and the model has been experimentally vetted. Finally, it has been shown that MPPT models based on linear controllers can be inadequate for this application.

Acknowledgment

The authors wish to acknowledge the following for their valuable contributions to this paper: SDSU students R. Bhandari, E. Grebel, and D. Schutz; C. Thompson of Xantrex, Inc.; and S. Atcitty, W. Bower, B. Boysen, D. King, and J. Stevens of Sandia National Laboratories. Sandia is a multiprogram laboratory operated by Sandia Corporation, a Lockheed Martin Company, for the United States Department of Energy's National Nuclear Security Administration under contract DE-AC04-94AL85000.

References

[1] M. E. Ropp, M. Begovic, and A. Rohatgi, "Prevention of islanding in grid-connected photovoltaic systems," *Prog. Photovolt.*, vol. 7, no. 1, pp. 39–59, 1999.

[2] W. Bower and M. Ropp, "Evaluation of islanding detection methods for utility-interactive inverters in photovoltaic systems," Sandia Nat. Lab., Albuquerque, NM, Rep. SAND2002-3591, Nov. 2002.

[3] *IEEE Standard for Interconnecting Distributed Resources with Electric Power Systems*, IEEE Standard 1547-2003, Jul. 28, 2003.

[4] *Inverters, Converters, and Controllers for Use in Independent Power Systems*, Underwriters' Laboratories Standard UL-1741, Standard for Safety, May 1999.

[5] *International Electrotechnical Commission TC82 working document, IEC-62116 "Test Procedure of Islanding Prevention Measures for Utility-Interconnected Photovoltaic Inverters" revised*, Sep. 29, 2006.

[6] M. Ropp, J. Ginn, J. Stevens, W. Bower, and S. Gonzalez, "Simulation and experimental study of the impedance detection anti-islanding method in the single-inverter case," in *Proc. 4th World Conf. Photovolt. Energy Convers.*, May 2006, pp. 2379–2382.

[7] F. Fernandez-Bernal, L. Rouco, P. Centeno, M. Gonzalez, and M. Alonao, "Modelling of photovoltaic plants for power system dynamic studies," in *Proc. 5th IEEE Int. Conf. Power Syst. Manage. Control*, 17–19 Apr. 2002, pp. 341–346.

[8] M. Ciobotaru, T. Kerekes, R. Teodorescu, and A. Bouscayrol, "PV inverter simulation using MATLAB/Simulink graphical environment and PLECS blockset," in *Proc. 32nd IEEE Ind. Electron. Conf.*, Paris, France, Nov. 2006, pp. 5313–5318.

[9] Z. Ye, R. Walling, L. Garces, R. Zhou, L. Li, and T. Wang, "Study and development of anti-islanding control for grid-connected inverters," Nat. Renewable Energy Lab, Golden, CO, May 2004, Rep. SR-560-36243, May 2004.

[10] M. Ropp, M. Begovic, and A. Rohatgi, "Analysis and performance assessment of the active frequency drift method of islanding prevention," *IEEE Trans. Energy Convers.*, vol. 14, no. 3, pp. 810–816, Sep. 1999.

[11] R. A. Jones and T. R. Sims, "Investigation of potential islanding of distributed photovoltaic systems," Sandia Nat. Lab., Albuquerque, NM, Rep. SAND-87-7024, 1988.

[12] A. Cocconi, S. Çuk, R. D. Middlebrook, and T. S. Key, "Design and development of a 4-kW/20 kHz DC-isolated power conditioner for utility interactive photovoltaic applications," Sandia Nat. Lab., Albuquerque, NM, Rep. SAND-87-0353, 1983.

[13] C. M. Alfonso, W. Freitas, W. Xu, and L. C. P. da Silva, "Performance of ROCOF relays for embedded generation applications," *Inst. Electr. Eng. Proc. Gener., Transmiss., Distrib.*, vol. 152, no. 1, pp. 109–114, Jan. 2005.

[14] D. Hohm and M. Ropp, "Comparative study of maximum power point tracking algorithms," *Prog. Photovolt.*, vol. 11, pp. 47–62, Jan. 2003.

[15] J. S. Arora, *Introduction to Optimum Design*. New York: McGraw-Hill, 1989.

[16] M. E. Ropp, M. Begovic, A. Rohatgi, G. A. Kern, R. Bonn, and S. Gonzalez, "Determining the relative effectiveness of islanding prevention techniques using phase criteria and nondetection zones," *IEEE Trans. Energy Convers.*, vol. 15, no. 3, pp. 290–296, Sep. 2000.

Michael E. Ropp (M'99) was born in Rapid City, SD, in 1967. He received the B.Sc. degree in music from the University of Nebraska-Lincoln, Lincoln, in 1992, and the M.S. and Ph.D. degrees in electrical engineering from the Georgia Institute of Technology, Atlanta, in 1996 and 1998, respectively.

He is an Associate Professor of electrical engineering at South Dakota State University, Brookings. His current research interests include issues relating to interfacing renewable energy systems to utility grids, power electronics for photovoltaics, distributed controls, and computer modeling of power systems.

Sigifredo Gonzalez received the M.S.E.E. degree from New Mexico State University, Las Cruces, in 1996.

He has been an Electrical Engineer of the Technical Staff, Sandia National Laboratories, Albuquerque, NM, for 11 years. His current research interests include performance, reliability, and utility interconnected standards compliance evaluations of photovoltaic dc/ac inverters.